Available online at www.sciencedirect.com

SciVerse ScienceDirect

Energy Procedia 15 (2012) 129 – 134

Energy Procedia

International Conference on Materials for Advanced Technologies 2011, Symposium O

Near-infrared Quantum Cutting in Eu^{3+}-Yb^{3+} co-doped YAG through Downconversion for Silicon Solar Cell

M.K. Lau and Jian-Hua Hao*

Department of Applied Physics and Materials Research Centre, The Hong Kong Polytechnic University, Hung Hom, Hong Kong

Abstract

Near-infrared (NIR) quantum cutting (QC) could provide a solution to minimise the heat loss due to the thermalisation of electron-hole pairs in solar cells by converting high-energy photons to low-energy photons matching with the greatest spectral response of silicon solar cell. Europium (Eu^{3+}) and ytterbium (Yb^{3+}) co-doped yttrium aluminium garnet ($Y_3Al_5O_{12}$, YAG) can be used as QC phosphor with emission in both visible and NIR regions. In this study, upon the excitation at 394 nm, the $^5D_0 \rightarrow 4f^6$ transition of Eu^{3+} is induced, the characteristic NIR emission located at 1030 nm due to the energy transfer between of $^2F_{5/2}$-$^2F_{7/2}$ levels of Yb^{3+}, is generated. The quantum efficiency (QE) was derived to be as high as 144%. The results showed the possibility for enhancing the photovoltaic conversion efficiency of silicon-based solar cell by modifying the absorption and utilising the energy in the UV-blue part of the solar spectrum.

Keywords: Fluoresent and luminescent materials; downconversion; rare-earth doped materials; infrared spectroscopy

1. Introduction

Efficient utilisation of solar energy has attracted global attention because the sun might be the source capable of generating sufficient energy to meet the long-term worldwide energy demand [1]. The concept of quantum cutting (QC) to generate two or more near-infrared (NIR) photons per incident high-energy photon has recently been explored in rare-earth (RE) materials. The investigative focus is presently on the study of a pair or even more RE ions dopants in single host. Yb^{3+} ion is usually a prime candidate to be

---

* Corresponding author. Tel.: +852 2766 4098; fax: +852 2333 7629
E-mail address: apjhhao@polyu.edu.hk

doi:10.1016/j.egypro.2012.02.015

chosen because its luminescent efficiency is close to 100% [2]. The energy of single excited level (~1.2 eV) is roughly in accordance with the band gap of silicon (~1.1 eV). If the downconversion is realised, the major energy loss due to thermalisation of hot charge carriers after the absorption of a high-energy photon in conventional silicon photovoltaic cells can be restrained. In the present study, yttrium aluminium garnet ($Y_3Al_5O_{12}$, YAG) is chosen. Energy transfer (ET) from Eu^{3+} to Yb^{3+} probably though a cooperative process is depicted in Fig. 1. Compared to the upconversion from Yb^{3+} to Eu^{3+} [3-6], the downconversion from Eu^{3+} to Yb^{3+} has rarely been studied. Here, we prepare Eu^{3+}-Yb^{3+} co-doped YAG by a conventional sol-gel method. The structural characterisations, visible and NIR emission, mean decay lifetimes and quantum efficiency (QE) of NIR QC, have been evaluated.

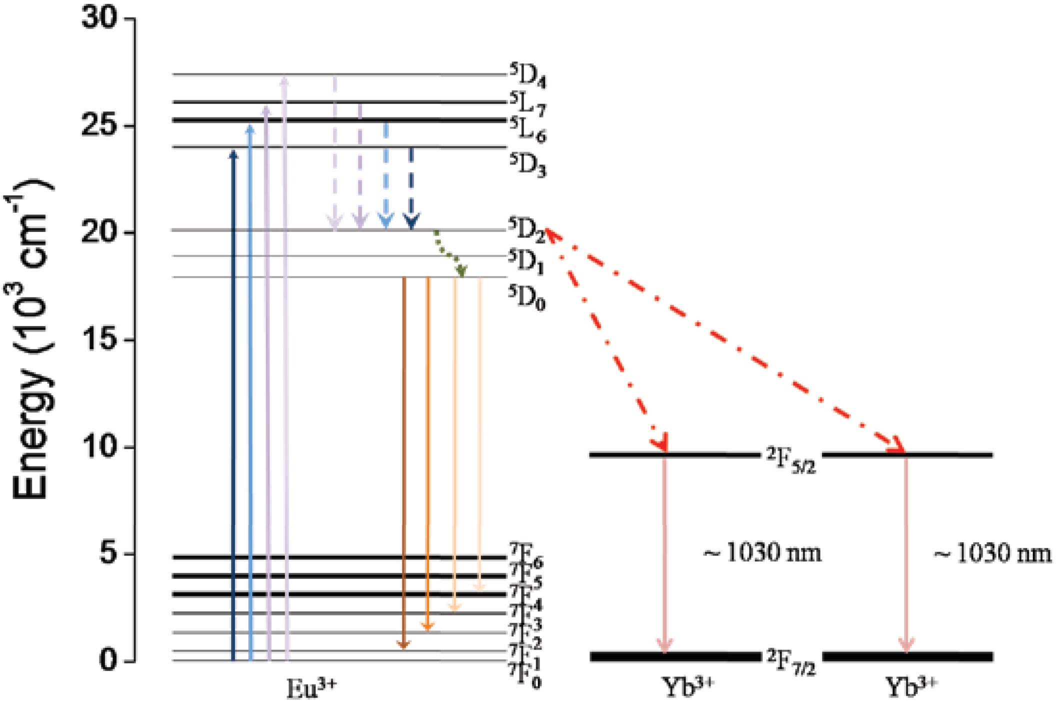

Fig. 1. Schematic energy level diagram of Eu^{3+}/Yb^{3+} co-doped YAG, illustrating the probable cooperative energy-transfer mechanism of NIR QC from $^5D_0$ level of Eu^{3+} to $^2F_{5/2}$ levels of Yb^{3+}. The solid arrows denoted the excitation and the emission processes. The dashed and dotted arrows represent non-radiative transition or energy-transfer processes.

2. Experimental

Y_2O_3, Yb_2O_3 and Eu_2O_3 were first dissolved in concentrated (69%) nitric acid and heated to evaporate excess acid with continuous stirring. Deionised water was added when the solution became gel-like, then it was placed in an oven at 80 ºC until it was completely dried. Al_2O_3, citric acid, deionised water and ethanol were added in stoichiometric proportions with constant stirring, and then annealed in oven at 80 ºC until the mixture was dried completely. The mixture was heated up to 550 ºC for 4 hours. It was milled into powder form and annealed to 1000 ºC for 4 hours. X-ray diffraction (XRD) was carried out to determine the crystal structure and identify the phase by the use of Bruker D8 Advance X-ray diffractometer, which operated at 40 kV and 40 mA, with Cu K_α radiation (λ = 0.15406 nm). The photoluminescence (PL) decay curves, excitation and emission spectra were accomplished at room temperature with a FLSP920 Edinburgh Analytical Instruments apparatus equipped with a 450 W xenon lamp.

3. Results and discussion

Figure 2 shows the XRD pattern of the YAG: Eu^{3+} and YAG: Eu^{3+}, Yb^{3+} powder. The structure and phase of the phosphors were confirmed and analysed. The doping concentration of Eu^{3+} and Yb^{3+} in YAG: Eu^{3+}, Yb^{3+} particles are 3 mol% and 5 mol%, respectively, if it is not denoted. The XRD data indicate that YAG: Eu^{3+} and YAG: Eu^{3+}, Yb^{3+} are basically in agreement with the structure known from bulk YAG [7], which is cubic phase with space group *Ia3d* (O_h^{10}) [8] and lattice parameter $a = 12.004$ Å.

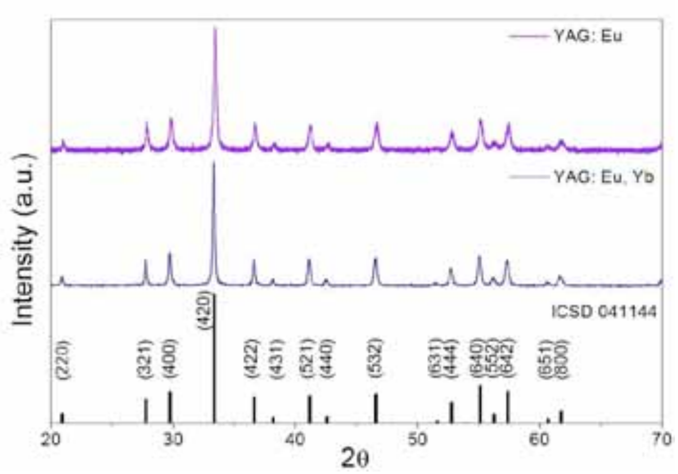

Fig. 2. XRD profiles of YAG: Eu^{3+} and YAG: Eu^{3+}, Yb^{3+}; the bars represent the diffraction pattern of the standard YAG phase.

Figure 3 shows the PLE spectra monitored 591 and 1030 nm. The excitation band ranging from 360 to 420 nm is ascribed to the $4f^6$ intraconfigurational transitions of Eu^{3+}, including $^7F_0 \rightarrow {}^5D_4$, $^7F_0 \rightarrow {}^5D_7$, $^7F_0 \rightarrow {}^5L_6$ and $^7F_0 \rightarrow {}^5D_3$. The absorption is followed by a rapid multi-phonon assisted relaxation from these populated levels to $^5D_2$ and finally the metastable state $^5D_0$ as presented in Fig. 1. The O^{2-}-Eu^{3+} charge transfer accounts for the excitation peak centered at 243 nm. Besides, the peak at 272 nm that appeared only in the excitation spectrum for the 1030 nm emission of Yb^{3+} is originated from an electron transfer from the ligand anion O^{2-} to Yb^{3+}, the position of which is close to the previous results of Yb^{3+} doped glasses reported on [9]. The energy mismatch between the lowest $^5D_0$ level of Eu^{3+} and the $^2F_{5/2}$ level of Yb^{3+} in the host of YAG is 8300 cm^{-1}, which is far larger than the vibration energy of the host. On the other hand, the Eu^{3+}: $^7F_0 \rightarrow {}^5D_2$ is located at approximately twice the energy of the Yb^{3+}: $^2F_{5/2} \rightarrow {}^2F_{7/2}$ transition and Yb^{3+} has no other levels up to the UV region. Nevertheless, the intensities of all the emission peaks in the visible range are consistently reduced by 46% for the Eu^{3+}-Yb^{3+} codoped YAG in comparison to the Eu^{3+} singly doped one, which can be considered that ET from Eu^{3+} to Yb^{3+} is the dominant mechanism to achieve NIR emission.

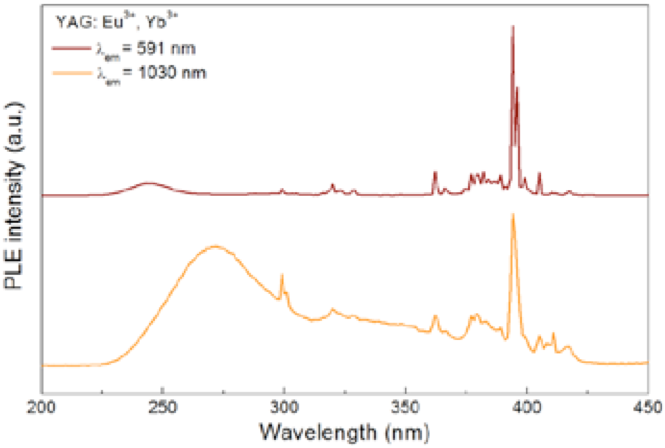

Fig. 3. PLE spectra of Eu^{3+} emission and Yb^{3+} emission of YAG: Eu^{3+}, Yb^{3+}

With 394 nm excitation, the emission spectrum of YAG: Eu^{3+}, Yb^{3+} shows a series of emission bands in the visible range which can be seen in Fig. 4, owing to the $^5D_0 \rightarrow {}^7F_J$ (J = 1, 2, 3, 4) of the $4f^6$ configuration of Eu^{3+} and a characteristic NIR emission peaked at 1030 nm associated with several weak shoulders (present in Fig. 5) attributed to the ET between $^2F_{5/2}$-$^2F_{7/2}$ levels of Yb^{3+}. Apart from the dominant peak located at 591 nm due to the $^5D_0 \rightarrow {}^7F_1$ transition of Eu^{3+}, some minor peaks are also observed at 596, 610, 630, 650, 655, 696, 701 and 710 nm. The splitting of the Stark components ^7F_J by the crystal field induces the additional spectral lines. The absence of $^5D_0 \rightarrow {}^7F_0$ demonstrates that Eu^{3+} ions occupied the centrosymmetrical site in YAG lattice. The hypersensitive transition $^5D_0 \rightarrow {}^7F_2$ hence becomes suppressed.

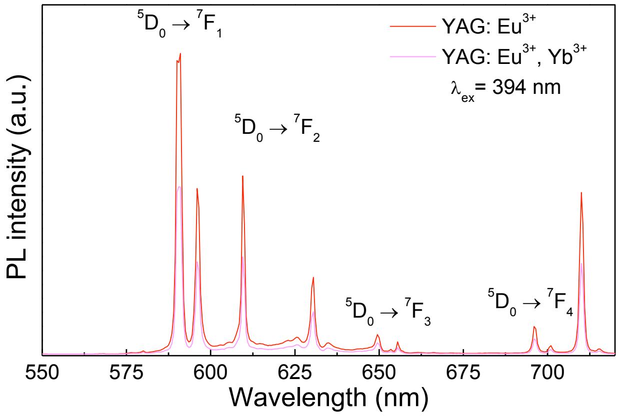

Fig. 4. PL spectra in the visible range of YAG: Eu^{3+} and YAG: Eu^{3+}, Yb^{3+}

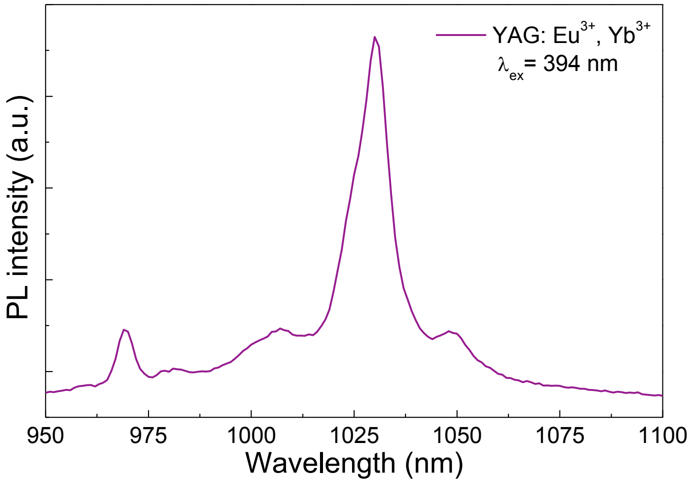

Fig. 5. PL spectrum in the NIR range of YAG: Eu^{3+}, Yb^{3+}

The dynamics of Eu^{3+} ($^5D_0 \rightarrow {}^7F_1$) photoluminescence upon excitation with a photon at 394 nm is presented in Fig. 6. The decay curve of Eu^{3+} singly doped phosphor exhibits a nearly first-order exponential with a lifetime of 3.91 ms. However, the decay curve becomes non-exponential and the decay rate increases rapidly when Yb^{3+} is added. This phenomenon further clarifies the possibility of cooperative ET from Eu^{3+} to Yb^{3+}.

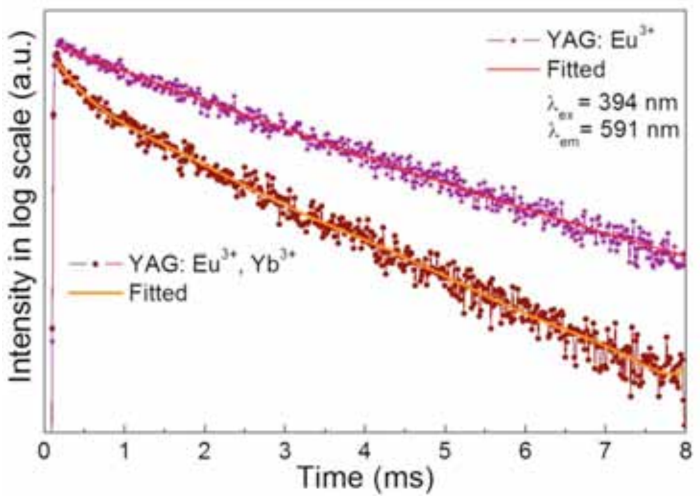

Fig. 6. Decay curves corresponding to the Eu^{3+} transition of YAG: Eu^{3+} and YAG: Eu^{3+}, Yb^{3+}

From Fig. 6, the ET efficiency (η_{ET}) and the internal QE (η_{QE}) can be determined by the equations according to the framework of a cooperative DC model [10].

$$\eta_{ET} = 1 - \frac{\int I_{x\%Yb}dt}{\int I_{0\%Yb}dt}, \tag{1}$$

$$\eta_{QE} = \eta_{Eu}(1-\eta_{ET}) + 2\eta_{Yb}\eta_{ET}, \tag{2}$$

where I represents the luminescence intensity at time t and $x\%$ Yb denotes the concentration in mol%. η_{Eu} and η_{Yb} are the QE of $\mathrm{Eu^{3+}}$ and $\mathrm{Yb^{3+}}$, respectively, both of them are set to unity if ideal quantum cutting occurred. The internal QE of 144% is determined for the $\mathrm{Eu^{3+}}$-$\mathrm{Yb^{3+}}$ co-doped YAG, this value represents that 144 NIR and visible photons will be produced upon absorption of 100 photons at 394 nm, of which 88 photons are emitted at 960-1060 nm. However, the actual QE may be lower than the internal QE when the concentration quenching and phonon-assisted non-radiative process are taken into account.

4. Conclusion

The excitation bands of the phosphors are within the region of spectral response of silicon solar cell while the emission peak at 1030 nm refers to the greatest spectral response. Energy transfer occurs from $\mathrm{Eu^{3+}}$ to sensitised $\mathrm{Yb^{3+}}$ in YAG. The obtained results have potential application values in the field of silicon photovoltaics.

Acknowledgements

This work was supported by the Hong Kong Polytechnic University Postgraduate Scholarship (RPAQ) and Internal Grant (A-PK07). The authors acknowledge Mr S.T.F. Lee, Mr C.M. Luk and Mr Z.H. Sun for their technical assistance.

References

[1] Van der Ende MB, Aarts L, Meijerink A. Near-infrared quantum cutting for photovoltaics. *Adv. Mater.* 2009; **21(30)**: 3037-3128.

[2] Ueda J, Tanabe S. Visible to near infrared conversion in $\mathrm{Ce^{3+}}$-$\mathrm{Yb^{3+}}$ co-doped YAG ceramics. *J. Appl. Phys.* 2009; **106**:043101.

[3] Wei X, Zhao J, Zhang W, Li Y, Yin M. Cooperative energy transfer in $\mathrm{Eu^{3+}}$, $\mathrm{Yb^{3+}}$ codoped $\mathrm{Y_2O_3}$ phosphor. *J. Rare Earths* 2010; **28**:166.

[4] Dwivedi Y, Thakur SN, Rai SB. Study of frequency upconversion by cooperative energy transfer in oxyfluoroborate glass matrix. *Appl. Phys. B* 2007; **89**:45-51.

[5] Yang CH, Yang GF, Pan YX, Zhang QY. Synthesis and spectroscopic properties of $\mathrm{GdAl_3(BO_3)_4}$ poly-crystals codoped with $\mathrm{Yb^{3+}}$ and $\mathrm{Eu^{3+}}$. *J. Fluoresc.* 2009; **19**:105-109.

[6] Maciel GS, Biswas A, Prasad PN. Infrared-to-visible $\mathrm{Eu^{3+}}$ energy upconversion due to cooperative energy transfer from an $\mathrm{Yb^{3+}}$ ion pair in a sol-ge; processed multi-component silica glass. *Opt. Commun.* 2000; **178**:65-9.

[7] Bagdasarov KHS, Bolotina NB, Kalinin VI, Karyagin VF, Kuz'min BV, Muradyan LA *et al.* Photoinduced effects and real structure of yttrium-aluminum garnet crystals. *Kristallografiya* 1991; **36**: 715-28.

[8] Gross H, Neukum J, Heber J, Materika D, Tang X. Crystal-field analysis of $\mathrm{Eu^{3+}}$-doped yttrium aluminium garnet by site-selective polarized spectroscopy. *Phys. Rev. B* 1993; **48**:9264-72.

[9] Liu X, Ye S, Qiao Y, Dong G, Zhu B, Chen D, Lakshminarayana G, Qiu J. Cooperative downconversion and near-infrared luminescence of $\mathrm{Tb^{3+}}$-$\mathrm{Yb^{3+}}$ codoped lanthanum borogermanate glasses. *Appl. Phys. B* 2009; **96**:51-5.

[10] Vergeer P, Vlugt TJH, Kox MHF, den Hertog MI, van der Eerden JPJM, Meijerink A. Quantum cutting by cooperative energy transfer in $\mathrm{Yb_xY_{1-x}PO_4}$: $\mathrm{Tb^{3+}}$. *Phys. Rev. B* 2005; **71**:014119.